Published in final edited form as:
Nanomedicine (Lond). 2011 February ; 6(2): 351–364. doi:10.2217/nnm.10.136.

Cowpea mosaic virus nanoparticles target surface vimentin on cancer cells

Nicole F Steinmetz[1,2], **Choi-Fong Cho**[3,4], **Amber Ablack**[3], **John D Lewis**[3,4], and **Marianne Manchester**[1,†]

[1] Department for Cell Biology, Center for Integrative Molecular Biosciences, The Scripps Research Institute, La Jolla, CA, USA

[2] Department of Biomedical Engineering, Case Center for Imaging Research, Case Western Reserve University, Cleveland, OH, USA

[3] Translational Prostate Cancer Research Group, London Regional Cancer Program, London, ON, Canada

[4] Department of Medical Biophysics, University of Western Ontario, London, ON, Canada

Abstract

Aims—Vimentin, a type III intermediate filament, is upregulated during epithelial–mesenchymal transition and tumor progression. Vimentin is surface-expressed on cells involved in inflammation; the function remains unknown. We investigated the expression of surface vimentin on cancer cells and evaluated targeting nanoparticles to tumors exploiting vimentin.

Materials & methods—Cowpea mosaic virus nanoparticles that interact with surface vimentin were used as probes. Tumor homing was tested using the chick chorioallantoic membrane model with human tumor xenografts.

Results & discussion—Surface vimentin levels varied during cell cycle and among the cell lines tested. Surface vimentin expression correlated with cowpea mosaic virus uptake, underscoring the utility of cowpea mosaic virus to detect invasive cancer cells. Targeting to tumor xenografts was observed; homing was based on the enhanced permeability and retention effect. Our data provide novel insights into the role of surface vimentin in cancer and targeting nanoparticles *in vivo*.

Keywords

CAM model; cancer; cell cycle; CPMV; EPR effects; PEGylation; vimentin; viral nanoparticles

†Author for correspondence: Skaggs School of Pharmacy & Pharmaceutical Sciences, University of California San Diego, La Jolla, CA 92093, USA, Tel.: +1 858 534 6624, Fax: +1 858 822 7709, mmanchester@ucsd.edu.

No writing assistance was utilized in the production of this manuscript.

Ethical conduct of research

The authors state that they have obtained appropriate institutional review board approval or have followed the principles outlined in the Declaration of Helsinki for all human or animal experimental investigations. In addition, for investigations involving human subjects, informed consent has been obtained from the participants involved.

Financial & competing interests disclosure

This study was supported by an American Heart Association Postdoctoral Fellowship (to Nicole F Steinmetz), NIH grants K99 EB009105 (to Nicole F Steinmetz) and R01 CA112075 (to Marianne Manchester), and by CIHR MOP-84535 grant (to John D Lewis). The authors have no other relevant affiliations or financial involvement with any organization or entity with a financial interest in or financial conflict with the subject matter or materials discussed in the manuscript apart from those disclosed.

The recent advent of nanotechnology in combination with the identification of tumor markers and their ligands has opened the door for the development of targeted imaging modalities for cancer detection and agents for treatment [1,2]. Gaining understanding of tumor architecture to help identify tumor markers with potential for targeting applications is an important objective in biomedicine. One interesting potential tumor marker is vimentin [3].

Vimentin is a type III intermediate filament that is predominantly expressed in the cytoplasm in cells of mesenchymal origin. Vimentin is the only intermediate filament expressed in a large variety of cells, including fibroblasts, endothelial cells, macrophages, neutrophils and lymphocytes. Cytosolic vimentin is a key component of the cytoskeleton, and plays a role in a variety of fundamental cellular processes, such as wound healing, cell–cell physical interactions, motility, contraction, migration, proliferation, protein synthesis, gene expression, apoptosis and signal transduction [3,4]. Cytosolic vimentin also plays a role in cell adhesion in migrating cells, and is a component of the vimentin-associated matrix adhesion complex [5–8], suggesting a role in tumor metastasis.

There is growing evidence of an association between vimentin expression and tumor development and progression. As a marker of cells of mesenchymal origin, vimentin is thought to be a key player in the epithelial–mesenchymal transition (EMT), a hallmark of tumor invasiveness and aggressiveness [3]. Vimentin overexpression is also linked to poor clinical prognosis for cancer patients. A role of vimentin in the growth and invasiveness of cancer cells has been indicated for a number of cancers, including those of breast, prostate, colon and osteosarcomas [9–13].

In addition to its cytosolic localization, vimentin has recently been identified as a surface-exposed and/or secreted protein in activated macrophages [14], T lymphocytes [15], Sezary T cells [15], apoptotic neutrophils [16], endothelial cells, specifically in tumor tissue [17–19], and endothelial venules of lymph nodes [18]. The mechanism by which surface vimentin translocates from the cytosol to the plasma membrane is unknown. Based on the expression pattern of surface vimentin it has been suggested that the protein may mediate endothelial interactions with blood circulating cells and migrating cells, or may participate in the formation of an anchoring structure [5–8]. Surface and secreted forms of vimentin are overexpressed on endothelial cells of tumor tissue [17–19], and a role for surface vimentin in angiogenesis has been proposed [17]. Nevertheless, only very limited knowledge is available about the potential biological function of surface vimentin in cancers.

The expression pattern and function of surface vimentin on cancer cells themselves has not been extensively evaluated. To begin to study this, we made use of a novel viral nanoparticle (VNP) technology to exploit the plant VNP cowpea mosaic virus (CPMV) as a probe. CPMV as a tool has been extensively studied and applied for potential applications in materials science and biomedicine [20]. CPMV nanoparticles are monodisperse and approximately 30 nm in diameter (Figure 1). The *in vivo* properties of CPMV are well understood; after intravenous inoculation, CPMV particles are cleared rapidly from circulation with no apparent toxicity or pathological effects [21]. The use of fluorescent-labeled CPMV probes for intravital imaging has already been demonstrated. It was found that CPMV nanoparticles were internalized by endothelial cells *in vivo*, resulting in high-resolution labeling of vasculature, especially in tumor tissue [22]. Importantly, internalization of CPMV into endothelial cells and other cell types is mediated by cell surface-expressed vimentin [23,24]. This was previously demonstrated by direct binding assays to vimentin protein, inhibition of CPMV binding and entry into cells by vimentin-specific antibodies, and inhibition of CPMV entry into cells using vimentin-knockout cell lines [24].

The identification of a CPMV–vimentin interaction opened the door for us to utilize the plant VNP as a tool to study the surface expression pattern of vimentin. We aimed to gain novel insights into the potential biological roles of the surface-expressed form of vimentin. The potential also exists to utilize CPMV to target tumor vasculature and cancer cells expressing surface vimentin. Cytosolic vimentin, along with other cytoskeletal proteins, can play a role during mitosis. The fate of the cytosolic organization of vimentin during mitosis is cell specific. For example, vimentin disassembles and recycles during mitosis in BHK-21 cells [25], whereas in endothelial cells as well as in HeLa cells vimentin retains filamentous continuity during mitosis [26–28]. Here, we specifically addressed the question as to whether the surface expression of vimentin varies at different stages of the cell cycle. In this study, we first studied the surface versus total cellular expression levels of vimentin during the cell cycle using HeLa cells, as the cell cycle of this cell line is well characterized [29].

We also analyzed the expression pattern of surface vimentin in comparison to cytosolic vimentin on various human cancer cell lines: HeLa (cervical cancer), MCF-7 and MDA-MB-231 (both breast cancer cell lines), and HT-29 (colon cancer). Others have shown that these cell lines vary in their tumorigenic potential and express varying levels of cytosolic vimentin [10,30–36].

Finally, we examined whether CPMV particles would preferentially localize in tumor tissue based on their specificity for vimentin. The uptake of CPMV and PEGylated CPMV particles (P2) were evaluated using human HT-29 tumor xenografts in the chick chorioallantoic membrane (CAM) model.

Materials & methods

Cell lines

Cell lines were obtained from ATCC (Manassas, VA, USA). Tissue culture reagents were purchased from Invitrogen (Carlsbad, CA, USA). HeLa cells were grown in DMEM or MEM with 7% fetal bovine serum (FBS), 1% L-glutamine, and 1% penicillin–streptomycin (PS). MCF-7 cells were grown in MEM with 10% FBS, 1% L-glutamine and 1% PS. MDA-MB-231 were grown in DMEM with 10% FBS, 1% L-glutamine, 1% sodium pyruvate and 1% PS. HT-29 cells were grown in RPMI with 10% FBS, 1% L-glutamine and 1% PS. Cells were incubated at 37°C and 5% CO_2.

Virus propagation & purification

Cowpea mosaic virus was propagated in *Vigna unguiculata* and purified using established procedures [37].

Chemical attachment of PEG2000 & O488 or A647

PEG2000, Oregon Green 488 (O488) and/or Alexa Fluor 647 (A647) were covalently attached to surface Lys residues on CPMV using *N*-hydroxysuccinimide (NHS)-activated esters. PEG2000–NHS (NANOCS, New York, NY), O488–NHS (*6 isomer*), or A647–NHS (Invitrogen) was dissolved in DMSO and added to CPMV in a molar excess of 3000 to CPMV (2–3 mg ml^{-1}), and the reaction was carried out for 2 h or overnight at room temperature in a phosphate buffered saline (PBS) pH 7.2:DMSO mixture of 8:2. Samples were purified using gradient ultracentrifugation in 10–40% sucrose gradients in 0.1 M phosphate buffer pH 7.0 (Beckman SW 28 Ti rotor, 28700 rpm, 3 h, 4°C) followed by ultra-pelleting (Beckman 50.2 Ti rotor, 42000 rpm, 3 h, 4°C). Alternatively, samples were purified via dialysis using 100K cut-off centrifugal devices (Millipore, Billerica, MA, USA). CPMV was resuspended in PBS pH 7.2 and stored at 4°C. CPMV formulations labeled with PEG2000 are referred to as P2, dye-labeled and double-labeled constructs are referred to as

CPMV–O488, CPMV–A647, P2–O488 and P2–A647. Particles were analyzed by size-exclusion chromatography (SEC), gel electrophoresis and transmission electron microscopy (TEM), as described below.

Size exclusion chromatography

All labeled particles were analyzed on a Superose6 column using the ÄKTA Explorer (GE Healthcare). Concentrated samples (500 μl of 0.2 mg ml^{-1}) were analyzed at a flow rate of 0.5 mg ml^{-1}, using 0.1 M potassium phosphate buffer pH 7.0.

Gel electrophoresis

Cowpea mosaic virus, CPMV–O488, P2, P2–O488, CPMV–A647 and P2–A647 particles were analyzed on native and denaturing gels. A total of 20 μg of sample (in loading dye, MBI Fermentas, Burlington, ON, Canada) was analyzed on 1.2% (w/v) agarose gel in 1 × TBE buffer, running buffer was 0.5× TBE (5 × TBE = 53 g of Tris base, 27.5 g boric acid, 20 ml 0.5 M EDTA pH 8.0 in 1 l MilliQ water). Protein subunits were analyzed on denaturing 4–12% NuPAGE® gels (Invitrogen) using 1× MOPS buffer (Invitrogen). 20 μg of sample (added LDS loading buffer; Invitrogen) was analyzed. After completion of the electrophoretic separation, the particles and protein subunits, respectively, were visualized under UV light or stained using Coomassie Blue. Photographs of the gels and the densitometry measurements were prepared using FluorChem™ SP imaging system.

Transmission electron microscopy

Cowpea mosaic virus particles (4–5 μl, ~1 mg/ml) were applied to continuous carbon grids (Ted Pella, Redding, CA, USA), which were washed three times with 100 μl of deionized water, then stained with 4 μl of 2% (w/v) uranyl acetate. Images were collected on Kodak film with a CM100 electron microscope at 53,000 magnification and scanned at 605 dpi using a Fuji FineScan 2750 × l (Hempel Hempstead, Herts, UK).

Surface & total vimentin staining by flow cytometry analysis

Cells were collected using Enzyme-free Cell Dissociation Buffer (Gibco/Invitrogen) and distributed in 200-μl portions at a concentration of 5×10^6 cells/ml in 96-well V-bottom shaped plates. To stain for cell surface vimentin, nonpermeabilized cells were stained with the mouse monocolonal antivimentin-specific antibody v9 (Sigma, St Louis, MO, USA). v9 was used at a dilution of 1:1000 in FACS buffer (PBS pH 7.4 containing 1 mM EDTA pH 8.0, 25 mM HEPES pH 7.5 and 1% FBS) and incubated at 4°C for 60 min. A secondary goat antimouse antibody conjugated to A647 was used at 1:2000 dilution in FACS buffer and incubated at 4°C for 60 min. Cells were either fixed with 2% formaldehyde for 15 min at room temperature prior to staining or live cell staining was performed.

To determine for total vimentin (cytosolic and surface vimentin), cells were fixed and then permeabilized using 0.2% saponin in FACS buffer. Antibody staining was conducted in FACS buffer containing saponin. Cells were re-suspended and analyzed using a FACS Calibur instrument (BD Biosciences, Franklin Lakes, NJ, USA). At least 10,000 gated events were collected. Experiments were repeated at least twice with triplicates of each sample measured. Data were analyzed using FlowJo 8.6.3 software (Tree Star, Inc, Ashland, OR, USA).

CPMV & P2 binding & uptake studies using flow cytometry

Cells were collected as described above. CPMV or P2 were added to live cells at a concentration of 1×10^5 VNPs per cell and incubated in medium at 37°C for 1–4 h prior to fixing and permeabilization using 0.2% (w/v) saponin in FACS buffer (see above). Staining

for CPMV was achieved using a polyclonal anti-CPMV antibody (1:1000 in FACS buffer) followed by a goat antirabbit secondary antibody conjugated to A647 or A488 (1:2000 in FACS buffer). All steps were carried out at 4°C. Cells were assayed as described above.

Vimentin staining during cell cycle using HeLa cells

Nucleic acid content was stained using propidium iodide (Invitrogen). Live cells were stained for surface vimentin as described above. Cells were then fixed using ice-cold (−20°C) ethanol at 4°C overnight at 1×10^6 cells/ml. Nucleic acids were stained using 80 μg propidium iodide and 400 μg RNaseA in 2 ml PBS pH 7.2 for at least 1 h at room temperature. For total vimentin staining, cells were fixed with ethanol prior to staining as described above. Analysis was performed using a FACS Calibur instrument and FlowJo 8.6.3 software (see above). Cell cycle analysis was performed according to the Dean/Jett/Fox model using FlowJo. For cell synchronization experiments, HeLa cells were synchronized using a double thymidine block as previously described [29]. Briefly, thymidine blocks cells in the early S phase; after the second block, cells progress synchronously through G2 and the mitotic phase. Flow cytometry analysis was performed and cells were collected at the following times: t = 0 (S phase), t = 4 h (G2 phase), t = 6 h (M phase), t = 8 h (G1 phase) and t = 16 h (completion of the cell cycle). Cells were stained for vimentin, and CPMV uptake studies were performed as described above.

Surface & cytosolic vimentin staining by confocal microscopy

A total of 5×10^4 cells were grown in 35-mm glass bottom petri dishes (Matek, Ashland, MA, USA) overnight at 37°C and 5% CO_2 in 2 ml medium. Cytosolic vimentin staining was as follows:

- Cells were fixed using 3% paraformaldehyde, 0.3% glutaraldehyde, 1 mM $MgCl_2$ in PBS pH 7.2 for 5 min at room temperature;
- Cells were blocked with 5% goat serum in PBS for 60 min at room temperature;
- Cell membranes were stained using Alexa Fluor 555-labeled wheat germ agglutinin (WGA-A555);
- Cells were permeabilized using 0.2% Triton X-100 in PBS for 2 min at room temperature;
- Vimentin was stained using the v9 monoclonal antibody (1:100 in PBS containing 1% goat serum) and A555- or A647-labeled secondary goat antimouse antibodies (1:500), each antibody at room temperature for 60 min;
- Cell nuclei were stained using 4′,6-diamidino-2-phenylindole (DAPI; 1:7500 for 10 min at room temperature).

Staining of surface vimentin was as follows:

- Live cells were blocked with 5% goat serum (30 min on ice);
- Stained with v9 and secondary antibodies;
- Fixed;
- Cell membranes stained;
- Nuclei stained.

Slides were mounted using Vecta Shield mounting medium (Vector Laboratories, Burlingame, CA, USA). Sections were imaged using a Biorad 2100 confocal microscope with a 60× oil objective. Images were created using ImageJ software [101].

CPMV uptake studies by confocal microscopy

Cells were grown as described above. A total of 5 μg CPMV–O488 particles were added in growth media and cells were incubated at 37°C and 5% CO_2 for 3 h. Excess CPMV was removed and cells incubated for an additional 3 h in growth medium, prior to fixation, blocking, cell membrane staining, staining of the nuclei, mounting and imaging as described above.

In vivo tumor homing studies

Fertilized chicken eggs (McKinley Hatchery, St Mary's, ON, Canada) were incubated in a rotary incubator at 37°C with 70% humidity for 4 days before being removed from the shell and placed in covered dishes. On day 9 of development, HT-29 cells were injected as a bolus at a concentration of 1.0×10^7 cells/ml in the stroma of the CAM and allowed to grow for 6 days (to 5 mm). On day 15, tumor-bearing embryos were injected intravenously with 100 μl of 1 mg/ml fluorescein dextran (MW 70,000 Da, Invitrogen) to visualize tumors and surrounding vasculature. Embryos were then injected with 100 μl of 800 μg/ml of CPMV or P2. A total of 6 h after injection, tumors were excised from the embryo, washed in PBS and placed in a prefix solution (10% sucrose and 3.7% formalin in PBS) at 4°C overnight. Next, tumors were washed in PBS and frozen in optimal cutting temperature (Tissue Tek) on dry ice. Frozen sections (8 μm) were collected (Leica CM 3050 S cryostat) on histobond glass slides and mounted in Prolong Gold (Invitrogen) mounting media containing DAPI. The uptake of CPMV and P2 was quantified by calculating the mean fluorescence intensity within selected tumor or nontumor stromal regions using ImageJ version 1.42q and GraphPad Prism, version 4.03.

Results

Surface vimentin expression levels vary during the cell cycle

Since we and others had previously shown that cells within a population expressed varying levels of surface vimentin [15,23,38], we reasoned that surface display of vimentin might vary with the cell cycle. To begin to test for this, we first evaluated the percentage of the cells' surface expression of vimentin in a HeLa cell population. Surface versus total vimentin (accounts for surface and cytosolic vimentin) expression levels were determined in nonsynchronized HeLa cells using the vimentin-specific monoclonal antibody v9 and flow cytometry (Figure 2A). We found that surface vimentin expression only represents a small fraction of total cellular vimentin.

Next, we set out to determine if there are differences during different stages of the cell cycle. We used propidium iodide, a fluorescent dye that intercalates into nucleic acid to identify cells in G1, S and G2 phases (Figure 2B). Propidium iodide is a commonly used reagent to stain cell cycle; the dye is permeable for the cell membrane and intercalates into the nucleic acid. The intensity of the signal is directly proportional to the nucleic acid content. Vimentin staining for the different cell populations was evaluated and the statistical analysis is given in Figure 2C. We found that surface vimentin levels indeed varied during the different stages of the cell cycle, and it was upregulated during the S and G2 phases compared with G1 ($p < 0.005$ based on Student 2-tailed t-test). By contrast, total vimentin levels remained constant throughout the cell cycle.

To investigate the cyclic nature of surface vimentin expression levels in greater detail, HeLa cells were synchronized using a double thymidine block. This procedure blocks S phase, and upon release cells progress synchronously through the S phase (0–4 h), enter G2 phase (5–6 h), undergo a synchronous mitosis at 7–8 h and re-enter S phase after completion of one full cell cycle at 14–16 h [29]. Cells were collected at each time point and stained for surface

vimentin using either the v9 anti-vimentin antibody or CPMV nanoparticles, and analyzed by flow cytometry. Propidium iodide staining confirmed cell synchronization and progression through the cell cycle as predicted (not shown). Surface vimentin staining was high at the beginning of S (t = 0 h) but trended lower when measured at the end of S (t = 4 h). Higher expression levels were also detected at the end of G2 (5–6 h) just prior to M (Figure 2D). The finding is consistent with the flow cytometry data gating the G1, S and G2 populations (Figure 2C). Cells with surface vimentin expression as detected by antibody staining could take up CPMV nanoparticles (Figure 2D). Thus, CPMV particles can also target HeLa cells at different stages of the cells cycle. It is possible that other rapidly dividing tumor cells will be disproportionally targeted by CPMV particles.

Surface vimentin expression & CPMV uptake in tumor cell lines *in vitro*

To explore targeting CPMV nanoparticles to cancer cells, we analyzed four different cancer cell lines for total vimentin, surface vimentin and CPMV uptake using a combination of confocal microscopy and flow cytometry. Flow cytometry gives quantitative data and confocal microscopy allows visualization of vimentin staining (qualitative data). Among the cell lines tested, HeLa (cervical cancer), MDA-MB-231 (breast cancer) and HT-29 (colon cancer) cells were shown to be positive for cytosolic vimentin, whereas MCF-7 cells (breast cancer) were negative. Confocal microscopy and flow cytometry data were in good agreement (Figures 3 & 4). Cell lines positive for cytosolic vimentin were also found to express surface vimentin, although surface vimentin levels on the breast cancer cell line MDA-MB-231 were rather low, with flow cytometry showing that 8% of the cells had detectable levels of surface vimentin (Figure 3D). Surface vimentin was not detectable by confocal microscopy, which is slightly less sensitive than FACS for detecting surface vimentin (Figure 4B4–4B6). HeLa and HT-29 cells showed the highest levels of surface vimentin (Figure 3A & 3B). Confocal microscopy revealed a polarized localization pattern on these cells for surface vimentin (Figure 4A4–4A6 & 4C4–4C9) as we have previously noted on HeLa cells [38].

To correlate CPMV interactions with surface vimentin expression levels, CPMV targeting to cancer cells was studied *in vitro*. CPMV-specific antibodies were used to detect CPMV by flow cytometry, whereas fluorescent-labeled CPMV–O488 particles were utilized for confocal microscopy studies (the conjugated fluorophores did not alter the CPMV–vimentin specificity as shown in Supplementary Figure 1, see online www.futuremedicine.com/doi/suppl/10.2217/nnm.10.136). This further supports that confocal and flow cytometry data can be compared with each other. To confirm specificity, CPMV particles were conjugated to polyethylene glycol (PEG). PEGylation is an effective strategy to reduce biospecific interactions, and we recently demonstrated that CPMV particles covalently attached to PEG2000 (termed P2 formulation) were effectively shielded and vimentin-mediated cell interactions are significantly blocked [39] in time-frames up to 3 h. Nevertheless we also noted that, over longer time periods, cells eventually bound and internalized this formulation as well (Supplementary Figure 2)

CPMV–O488 and P2 formulations were made using established bioconjugation methods. *N*-hydroxysuccinimide esters of Oregon Green 488 (O488) or PEG2000 were covalently attached to solvent-exposed Lys side chains on CPMV. The integrity of chemically modified VNPs as well as covalent decoration with the labels was confirmed using size-exclusion chromatography, transmission electron microscopy, gel electrophoresis and UV/visible spectroscopy as previously described [39]. CPMV–O488 displayed 60 fluorophores per virion as determined using UV/visible spectroscopy (not shown). Native and denaturing gels confirmed attachment of PEG molecules, and band intensity profiles indicated that each CPMV particle was labeled with approximately 30 PEG molecules (not shown) [39].

Binding and internalization of the CPMV VNPs was confirmed in HeLa and HT-29 cells (Figure 3A & 3B & Figure 4D), which were shown to express cell surface vimentin. Uptake correlated well to the determined surface vimentin expression levels (Figure 3). By flow cytometry, approximately 34% of HeLa cells were positive for surface vimentin staining, and CPMV uptake was also found to be approximately 38%. Similarly for HT-29 cells, 15% of the cells are positive for surface vimentin staining and 17% of the cells showed detectable levels of internalized CPMV particles (Figure 3A & 3B). In stark contrast, MDA-MB-231 cells were found to express very low levels of surface vimentin and MCF-7 that had no detectable levels of vimentin; uptake of CPMV particles in these cells was not detected (Figure 3C & 3D). Thus, it appears that CPMV particles only specifically targeted cells that displayed a relatively high level of surface vimentin, and these results are in agreement with our previous studies showing that either knockout of the vimentin gene or vimentin-specific antibodies could block CPMV entry [24].

Interaction of CPMV with tumors *in vivo*

To investigate the interaction between CPMV and tumor vasculature or tumor cells *in vivo*, we evaluated the uptake of CPMV–A647 and P2–A647 in human tumor xenografts derived from HT-29 cells in our previously established chick CAM model to evaluate tumor growth and vascularization [22]. In this model, human tumor cell lines can be on-planted onto the CAM and result in vascularized tumors within a few days, after which circulation and localization of particles may be observed in real time and quantified. Based on the high *in vitro* expression pattern of surface vimentin, we reasoned that HT-29 tumors would be a good model to evaluate CPMV uptake. Tumor size and vascularity was determined by injecting the avian embryos intravenously with a low molecular weight FITC-dextran (MW 70,000 Da) and visualizing by intravital confocal microscopy (Figure 5A). Avian embryos bearing well-vascularized tumors greater than 5 mm were split into two groups and injected intravenously with either CPMV–A647 or P2–A647.

Consistent with our previous studies, CPMV–A647 was rapidly internalized by the vascular endothelium after inoculation, and within approximately 30 min was not apparent in circulation but was entirely associated with endothelial cells (Figure 5B). After 6 h, tumor and nontumor tissue was excised, sectioned and visualized using confocal microscopy (Figure 5B) and evaluated for CPMV localization. Uptake of CPMV–A647 was observed in the tumor (Figure 5B, top panels) with a tumor–stroma fluorescence ratio of 8.9 (Figure 5C). PEGylated CPMV (P2–A647) was internalized much more slowly after inoculation [22]. We observed, as a result, a substantially longer circulation time for P2–A647 compared with CPMV–A647, as determined by the persistence of A647 fluorescence in the circulating blood. Interestingly, although the P2–A647 particles avoided vascular endothelial cells, the uptake of P2–A647 was significantly higher in the HT-29 tumors than CPMV–A647, as evidenced by distinct membrane labeling of cells within the tumor (Figure 5B, lower panels) and a measured tumor–stroma ratio of 26.5 (Figure 5C). The ability of CPMV to localize in tumors is dependent upon increased vascular permeability, as these VNPs are too large to passively diffuse out of the vasculature [40]. Given the substantially weaker interaction of P2–A647 with HT-29 cells compared with CPMV–A647, this somewhat surprising result can most likely be attributed to the significantly longer circulation time of P2–A647.

Discussion

Surface vimentin levels are upregulated just prior to M phase in HeLa cells

The fate of surface-expressed vimentin during cell cycle has not previously been characterized, and our studies thus provide first insights into a potential role of surface vimentin during mitosis. Studying cytosolic and surface vimentin levels during the cell cycle

showed that surface vimentin levels are upregulated just prior to mitosis (Figure 2C & 2D). Based on the expression pattern of surface vimentin, it has been previsouly suggested that the protein may play a role in cell migration at sites of disease and inflammation, and that it may participate in the formation of an anchoring structure [41]. The potential exists that surface vimentin also plays a role in telophase of mitosis, supporting migration of the daughter cells.

During the process of cell division, the cytoplasmic and nuclear components are reorganized and partitioned into daughter cells, with cytoskeletal elements playing a central role. Microtubules and microfilaments undergo disassembly during mitosis and then reorganize into filamentous networks. The fate of intermediate filaments during mitosis, however, appears to be cell- and intermediate filament-specific [42]. The intermediate filaments vimentin and desmin completely disassemble and recycle during mitosis in BHK-21 cells [25], whereas in endothelial cells vimentin retains filamentous continuity during mitosis [26]. This was also observed in HeLa cells, where the vimentin network also remains intact but the keratin network disassembles [27,28].

The mechanism by which vimentin translocates from the cytosol to the plasma membrane is unknown. It has been shown that surface and cytosolic vimentin are expressed from the same gene and that post-translational modifications, such as phosphorylation, play a role in translocation to the cell surface [4,18,43]. Vimentin is phoshorylated during the cell cycle, and the phosphorylation state is highest during M phase. In cells in which vimentin dissociates during mitosis, the higher phosphorylation state is inherent with reorganization and disassembly of the protein [44]. In cells where vimentin remains filamentous during mitosis, including HeLa cells, partitioning of vimentin into the daughter cells is facilitated by highly localized phosphorylation and disassembly events, specifically mediated by PKC and Rho [45–47]. The higher phosphorylation state and localized disassembly is in good agreement with the higher expression levels of surface vimentin on the dividing HeLa cells during M phase, and further supports the hypothesis that surface-expressed vimentin may play a role in cell migration and adhesion.

Surface expression levels of vimentin on cancer cells

Vimentin is an intermediate filament and is typically expressed in cells of mesenchymal origin [48]. However, vimentin is thought to be a key player in EMT and is associated with tumor aggressiveness [3]. We have shown that cytosolic vimentin is expressed in the epithelial cancer cell lines HeLa, MDA-MB-231 and HT-29, consistent with findings previously reported [10,27,28,30,31]. Interestingly, overexpression of cytosolic vimentin in breast cancers also correlates with an invasive phenotype. This is in agreement with our studies, that the noninvasive MCF-7 cell line is vimentin-negative, whereas MDA-MB-231 cells, which are known to have an invasive phenotype, express vimentin [10,30–32].

Surface vimentin levels on cells may also correlate with their tumorigenic potential. While there have been no direct evaluations of the tumorigenicity of all four cell lines tested in our study with regard to the relative rates of tumor formation in mice, cell migration potential *in vitro* or metastasis formation, some comparisons have been made. HT-29 cells may be regarded as an aggressive and tumorigenic cell line, and we and others have found that the relative rate of tumor formation in nude mice is higher for HT-29 cells compared with MDA-MB-231 or HeLa cells (data not shown and [33]). By contrast, *in vitro* cell migration assays indicated that MDA-MB-231 cells have higher invasive potential versus HT-29 cells [34–36]. Nevertheless, for MDA-MB-231 cells, it has been shown that the cytosolic expression of vimentin correlates with the aggressiveness of the cell line when compared with vimentin-negative MCF-7 cells [10,30–32]. Although HeLa cells are extensively studied in the literature, we could not find any studies comparing tumorigenicity with any of

the breast cancer cells or HT-29 cells used in this study. The localization pattern of surface vimentin on HeLa and HT-29 cells is interesting and appears polarized (punctate) at the cell membrane (Figure 4A & 4C), a phenomenon that has also been observed for the Sezary cell line HuT-78 [15]. In order to further confirm whether surface vimentin levels specifically determine the aggressiveness of a tumor cell line, future studies will include studying the tumorigenic potential of various surface vimentin high/low/negative cell lines using *in vitro* cell migration assays and *in vivo* tumor induction studies.

Localization of CPMV & P2 within tumors

Our observations clearly show that CPMV interacts with tumor cells *in vitro* via a high affinity interaction with vimentin and that PEGylation of CPMV lowers this affinity significantly; P2–A647 formulations are taken up by cells only after longer time periods (Figure 4 & Supplementary Figure 2). We found that while CPMV–A647 is indeed taken up in vimentin-expressing HT-29 tumors *in vivo*, the uptake of P2–A647 was threefold higher than that of CPMV–A647. The membrane localization of P2–A647 within these tumors suggested that the binding was vimentin dependent. While the affinity of a ligand for its target is an important consideration for *in vivo* tumor uptake, several recent studies have demonstrated that lower-affinity ligands can have improved characteristics for tumor targeting when compared with high-affinity analogs [49]. The bioavailability of nanoparticles at the tumor site is heavily dependent upon the enhanced permeability and retention (EPR) effect [50]. The EPR effect is the result of increased vascular permeability and inefficient lymphatic drainage in tumors, which allows nanoparticles to cross endothelial fenestrations and accumulate in the tumor parenchyma. We have previously shown that while CPMV nanoparticles do not extravasate in healthy blood vessels, they will extravasate in tumors [40]. We surmise that the increased targeting and retention of P2–A647 in HT-29 tumors is dependent upon extravasation into the tumor via the EPR effect, and that this was driven substantially by the increased plasma half-life of P2–A647.

Conclusion

The use of CPMV nanoparticles could prove to be a powerful new agent to target cancers, especially targeting metastasis. VNPs, such as CPMV, have many appealing features that make them uniquely suited to applications in materials and biomedicine. VNPs are extremely robust, well studied, and can be tailored by genetic modification and chemical bioconjugation methods. Plant VNPs can be quickly and inexpensively produced in gram quantities, and are biocompatible and noninfectious for humans [51]. VNPs are also currently being developed for specific tumor-targeting applications; for example, *in vivo* tumor homing by targeting the vascular EGF receptor 1 has recently been demonstrated in a murine preclinical model [22,40,52–54].

Our findings indicate that CPMV VNPs interact with surface vimentin on tumor cells, and underscore their potential utility for characterizing and detecting tumor cells *in vitro* and *in vivo*. As a role for vimentin in extracellular matrix adhesion and migration has been suggested [5–8], it is interesting to speculate that CPMV nanoparticles could act as agents to target tumor cells with greater metastatic potential.

In vivo studies evaluating the tumor-targeting capabilities of CPMV in an HT-29 tumor xenograft model indicated that CPMV particles effectively homed to tumors, but that the extended plasma half-life of PEGylated CPMV was more important than the high affinity of native CPMV for maximal tumor uptake. Further characterization of the CPMV–tumor interaction *in vivo*, as well as comparison to VNPs targeted to other tumor-specific markers, is warranted and is likely to yield new insights into the development and treatment of solid tumors.

Acknowledgments

The authors would like to thank Todd Braciak (Torrey Pines Institute for Molecular Studies) for helpful discussions and editing the manuscript. The authors would also like to thank So-Hye Cho for TEM studies.

Bibliography

Papers of special note have been highlighted as:

- ■ of interest
- ■■ of considerable interest

1. Hajitou A, Pasqualini R, Arap W. Vascular targeting: recent advances and therapeutic perspectives. Trends Cardiovasc Med. 2006; 16:80–88. [PubMed: 16546688]
2. Heath JR, Davis ME. Nanotechnology and cancer. Annu Rev Med. 2008; 59:251–265. [PubMed: 17937588]
3. Kokkinos MI, Wafai R, Wong MK, et al. Vimentin and epithelial–mesenchymal transition in human breast cancer – observations *in vitro* and *in vivo*. Cells Tissues Organs. 2007; 185:191–203. [PubMed: 17587825]
4■■. Ivaska J, Pallari HM, Nevo J, Eriksson JE. Novel functions of vimentin in cell adhesion, migration, and signaling. Exp Cell Res. 2007; 313:2050–2062. Summarizes the roles and functions of vimentin. [PubMed: 17512929]
5. Gonzales M, Weksler B, Tsuruta D, et al. Structure and function of a vimentin-associated matrix adhesion in endothelial cells. Mol Biol Cell. 2001; 12:85–100. [PubMed: 11160825]
6. Nishida Y, Shibata K, Yamasaki M, Sato Y, Abe M. A possible role of vimentin on the cell surface for the activation of latent transforming growth factor-β. FEBS Lett. 2009; 583:308–312. [PubMed: 19121313]
7. Kim H, Nakamura F, Lee W, et al. Filamin A is required for vimentin-mediated cell adhesion and spreading. Am J Physiol Cell Physiol. 2009; 298(2):C221–C236. [PubMed: 19776392]
8. Bhattacharya R, Gonzalez AM, Debiase PJ, et al. Recruitment of vimentin to the cell surface by β3 integrin and plectin mediates adhesion strength. J Cell Sci. 2009; 122:1390–1400. [PubMed: 19366731]
9. McInroy L, Maatta A. Down-regulation of vimentin expression inhibits carcinoma cell migration and adhesion. Biochem Biophys Res Commun. 2007; 360:109–114. [PubMed: 17585878]
10. Nagaraja GM, Othman M, Fox BP, et al. Gene expression signatures and biomarkers of noninvasive and invasive breast cancer cells: comprehensive profiles by representational difference analysis, microarrays and proteomics. Oncogene. 2006; 25:2328–2338. [PubMed: 16314837]
11. Singh S, Sadacharan S, Su S, et al. Overexpression of vimentin: role in the invasive phenotype in an androgen-independent model of prostate cancer. Cancer Res. 2003; 63:2306–2311. [PubMed: 12727854]
12. Takemura K, Hirayama R, Hirokawa K, et al. Expression of vimentin in gastric cancer: a possible indicator for prognosis. Pathobiology. 1994; 62:149–154. [PubMed: 7945921]
13. Alfonso P, Nunez A, Madoz-Gurpide J, et al. Proteomic expression analysis of colorectal cancer by two-dimensional differential gel electrophoresis. Proteomics. 2005; 5:2602–2611. [PubMed: 15924290]
14. Mor-Vaknin N, Punturieri A, Sitwala K, Markovitz DM. Vimentin is secreted by activated macrophages. Nat Cell Biol. 2003; 5:59–63. [PubMed: 12483219]
15. Huet D, Bagot M, Loyaux D, et al. SC5 mAb represents a unique tool for the detection of extracellular vimentin as a specific marker of Sezary cells. J Immunol. 2006; 176:652–659. [PubMed: 16365461]
16. Moisan E, Girard D. Cell surface expression of intermediate filament proteins vimentin and lamin B1 in human neutrophil spontaneous apoptosis. J Leukoc Biol. 2006; 79:489–498. [PubMed: 16365157]

17■■. van Beijnum JR, Dings RP, van der Linden E, et al. Gene expression of tumor angiogenesis dissected: specific targeting of colon cancer angiogenic vasculature. Blood. 2006; 108:2339–2348. Demonstrates the feasibility of targeting of solid tumors *in vivo* using antivimentin specific antibodies. [PubMed: 16794251]

18. Xu B, deWaal RM, Mor-Vaknin N, et al. The endothelial cell-specific antibody PAL-E identifies a secreted form of vimentin in the blood vasculature. Mol Cell Biol. 2004; 24:9198–9206. [PubMed: 15456890]

19. Leenstra S, Das PK, Troost D, et al. PAL-E, monoclonal antibody with immunoreactivity for endothelium specific to brain tumours. Lancet. 1990; 335:671. [PubMed: 1969053]

20■. Steinmetz, NF.; Lin, T.; Lomonossoff, GP.; Johnson, JE. Structure-based engineering of an icosahedral virus for nanomedicine and nanotechnology. In: Manchester, M.; Steinmetz, NF., editors. Viruses and Nanotechnology. Springer Verlag; Berlin Heidelberg, Germany: 2008. p. 23-58.Summarizes the bioconjugation and potential applications of cowpea mosaic virus (CPMV) in nanotechnology

21■. Singh P, Prasuhn D, Yeh RM, et al. Bio-distribution, toxicity and pathology of cowpea mosaic virus nanoparticles *in vivo*. J Control Release. 2007; 120:41–50. Demonstrates the feasibility of using CPMV for *in vivo* applications; potential toxic side effects were not apparent after administration in mice. [PubMed: 17512998]

22■■. Lewis JD, Destito G, Zijlstra A, et al. Viral nanoparticles as tools for intravital vascular imaging. Nat Med. 2006; 12:354–360. Demonstrates the feasibility of fluorescent-labeled CPMV particles for imaging of the vasculature. [PubMed: 16501571]

23. Gonzalez MJ, Plummer EM, Rae CS, Manchester M. Interaction of cowpea mosaic virus (CPMV) nanoparticles with antigen presenting cells *in vitro* and *in vivo*. PLoS One. 2009; 4:E7981. [PubMed: 19956734]

24. Koudelka KJ, Destito G, Plummer EM, et al. Endothelial targeting of cowpea mosaic virus (CPMV) via surface vimentin. PLoS Pathog. 2009; 5:E1000417. [PubMed: 19412526]

25. Rosevear ER, McReynolds M, Goldman RD. Dynamic properties of intermediate filaments: disassembly and reassembly during mitosis in baby hamster kidney cells. Cell Motil Cytoskeleton. 1990; 17:150–166. [PubMed: 2268873]

26. Blose SH. Ten-nanometer filaments and mitosis: maintenance of structural continuity in dividing endothelial cells. Proc Natl Acad Sci USA. 1979; 76:3372–3376. [PubMed: 386339]

27. Jones JC, Goldman AE, Yang HY, Goldman RD. The organizational fate of intermediate filament networks in two epithelial cell types during mitosis. J Cell Biol. 1985; 100:93–102. [PubMed: 2578129]

28. Franke WW, Schmid E, Grund C, Geiger B. Intermediate filament proteins in nonfilamentous structures: transient disintegration and inclusion of subunit proteins in granular aggregates. Cell. 1982; 30:103–113. [PubMed: 6751555]

29. Whitfield ML, Sherlock G, Saldanha AJ, et al. Identification of genes periodically expressed in the human cell cycle and their expression in tumors. Mol Biol Cell. 2002; 13:1977–2000. [PubMed: 12058064]

30. Sommers CL, Byers SW, Thompson EW, Torri JA, Gelmann EP. Differentiation state and invasiveness of human breast cancer cell lines. Breast Cancer Res Treat. 1994; 31:325–335. [PubMed: 7881109]

31. Hendrix MJ, Seftor EA, Seftor RE, Trevor KT. Experimental co-expression of vimentin and keratin intermediate filaments in human breast cancer cells results in phenotypic interconversion and increased invasive behavior. Am J Pathol. 1997; 150:483–495. [PubMed: 9033265]

32. Brabletz T, Hlubek F, Spaderna S, et al. Invasion and metastasis in colorectal cancer: epithelial-mesenchymal transition, mesenchymal-epithelial transition, stem cells and β-catenin. Cells Tissues Organs. 2005; 179:56–65. [PubMed: 15942193]

33. Dkhissi F, Lu H, Soria C, et al. Endostatin exhibits a direct antitumor effect in addition to its antiangiogenic activity in colon cancer cells. Hum Gene Ther. 2003; 14:997–1008. [PubMed: 12869217]

34. Li BH, Yang XZ, Li PD, et al. IL-4/Stat6 activities correlate with apoptosis and metastasis in colon cancer cells. Biochem Biophys Res Commun. 2008; 369:554–560. [PubMed: 18294957]

35. Gohla A, Eckert K, Maurer HR. A rapid and sensitive fluorometric screening assay using YO-PRO-1 to quantify tumour cell invasion through Matrigel. Clin Exp Metastasis. 1996; 14:451–458. [PubMed: 8871539]

36. Joshi B, Strugnell SS, Goetz JG, et al. Phosphorylated caveolin-1 regulates Rho/ROCK-dependent focal adhesion dynamics and tumor cell migration and invasion. Cancer Res. 2008; 68:8210–8220. [PubMed: 18922892]

37. Wellink J. Comovirus isolation and RNA extraction. Meth Mol Biol. 1998; 81:205–209.

38■■. Koudelka KJ, Destito G, Plummer EM, et al. Endothelial targeting of cowpea mosaic virus via surface vimentin. PLoS Pathog. 2009; 5(5):E1000417. Surface vimentin is the CPMV-binding protein on mammalian cells. [PubMed: 19412526]

39■. Steinmetz NF, Manchester M. PEGylated viral nanoparticles for biomedicine: the impact of PEG chain length on VNP cell interactions *in vitro* and *ex vivo*. Biomacromolecules. 2009; 10(4):784–792. PEGylation of CPMV is an effective strategy to avoid natural CPMV–cell interactions. [PubMed: 19281149]

40■■. Brunel FM, Lewis JD, Destito G, et al. Hydrazone ligation strategy to assemble multifunctional viral nanoparticles for cell imaging and tumor targeting. Nano Lett. 2010; 10:1093–1097. *In vivo* tumor homing of CPMV particles targeted to the vascular EGF receptor 1. [PubMed: 20163184]

41. Nieminen M, Henttinen T, Merinen M, et al. Vimentin function in lymphocyte adhesion and transcellular migration. Nat Cell Biol. 2006; 8:156–162. [PubMed: 16429129]

42. Chou YH, Opal P, Quinlan RA, Goldman RD. The relative roles of specific N- and C-terminal phosphorylation sites in the disassembly of intermediate filament in mitotic BHK-21 cells. J Cell Sci. 1996; 109(Pt 4):817–826. [PubMed: 8718673]

43. Ivaska J, Vuoriluoto K, Huovinen T, et al. PKCε-mediated phosphorylation of vimentin controls integrin recycling and motility. EMBO J. 2005; 24:3834–3845. [PubMed: 16270034]

44. Chou YH, Rosevear E, Goldman RD. Phosphorylation and disassembly of intermediate filaments in mitotic cells. Proc Natl Acad Sci USA. 1989; 86:1885–1889. [PubMed: 2648386]

45. Goto H, Kosako H, Inagaki M. Regulation of intermediate filament organization during cytokinesis: possible roles of Rho-associated kinase. Microsc Res Tech. 2000; 49:173–182. [PubMed: 10816257]

46. Takai Y, Ingaki M. Visualization of site-specific phosphorylation of intermediate filaments during the cell cycle. Tanpakushitsu Kakusan Koso. 1996; 41:1920–1926. [PubMed: 8890656]

47. Yasui Y, Goto H, Matsui S, et al. Protein kinases required for segregation of vimentin filaments in mitotic process. Oncogene. 2001; 20:2868–2876. [PubMed: 11420699]

48. Evans RM. Vimentin: the conundrum of the intermediate filament gene family. Bioessays. 1998; 20:79–86. [PubMed: 9504050]

49. Gagnon MK, Hausner SH, Marik J, et al. High-throughput *in vivo* screening of targeted molecular imaging agents. Proc Natl Acad Sci USA. 2009; 106:17904–17909. [PubMed: 19815497]

50. Iyer AK, Khaled G, Fang J, Maeda H. Exploiting the enhanced permeability and retention effect for tumor targeting. Drug Discov Today. 2006; 11:812–818. [PubMed: 16935749]

51. Young M, Willits D, Uchida M, Douglas T. Plant viruses as biotemplates for materials and their use in nanotechnology. Annu Rev Phytopathol. 2008; 46:361–384. [PubMed: 18473700]

52. Destito G, Yeh R, Rae CS, Finn MG, Manchester M. Folic acid-mediated targeting of cowpea mosaic virus particles to tumor cells. Chem Biol. 2007; 14:1152–1162. [PubMed: 17961827]

53. Pasqualini R, Koivunen E, Ruoslahti E. α v integrins as receptors for tumor targeting by circulating ligands. Nat Biotechnol. 1997; 15:542–546. [PubMed: 9181576]

54. Suci PA, Berglund DL, Liepold L, et al. High-density targeting of a viral multifunctional nanoplatform to a pathogenic, biofilm-forming bacterium. Chem Biol. 2007; 14:387–398. [PubMed: 17462574]

Website

101. ImageJ. Download ImageJ 1.43 software. http://rsbweb.nih.gov/ij/download.html

Executive summary

- Surface vimentin expression levels are upregulated just prior to mitosis in HeLa cells. This further supports the hypothesis that surface-expressed vimentin may play a role in cell migration and adhesion.
- HeLa, MDA-MB-231 and HT-29 cells are vimentin-positive, MCF-7 cells are vimentin-negative.
- Surface vimentin expression levels were highest in HeLa and HT-29 cells; the degree of surface vimentin expression correlated with cowpear mosaic virus (CPMV) uptake.
- Surface vimentin expression appears polarized at the cell membrane.
- Data indicate that surface vimentin levels could correlate with the tumorigenic potential of tumor cells.
- Extending the plasma half-life of CPMV is critical to ensure maximal uptake in tumors *in vivo*.

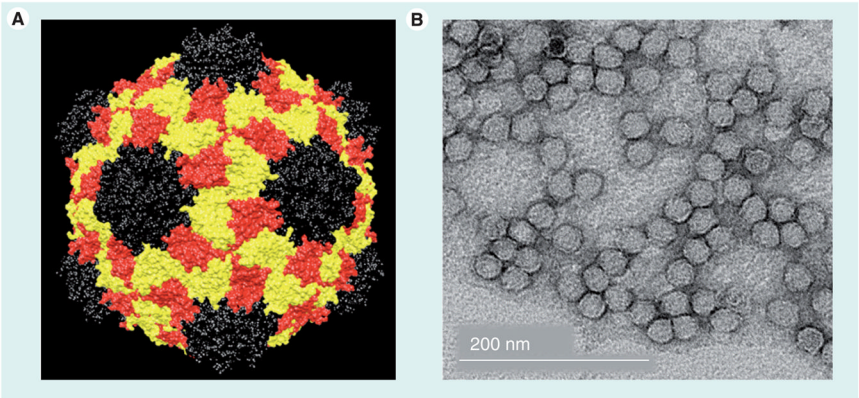

Figure 1. Cowpea mosaic virus nanoparticles

(A) Structure of the Cowpea mosaic virus (CPMV). The small coat protein is depicted in black; the two-domain large coat protein is shown in yellow and red. The image was created using Chimera, the coordinates were downloaded from the VIPER database (viperdb.scripps.edu; file 1NY7). **(B)** Transmission electron microscopy of negatively stained (2% w/v uranyl acetate) CPMV particles.

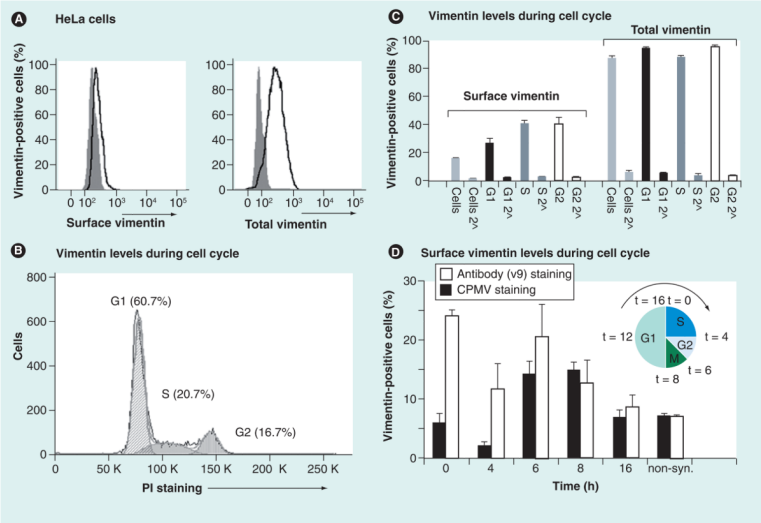

Figure 2. Surface vimentin expression during the cell cycle is regulated

(A) Expression levels of surface versus total vimentin on HeLa cells studied by flow cytometry. To stain for total vimentin, cells were permeabilized prior to staining. Gray solid histogram: secondary antibody only; black open histrogram: cells stained with v9, the vimentin-specific monoclonal antibody and secondary antibodies. **(B)** Cell cycle analysis of PI-stained cells. Analysis was performed using FlowJo 8.7.1 software; cell cycle analysis was according to the Dean/Jett/Fox model. Cells in G1, S and G2 phase were gated based on their DNA content, which is directly proportional to the intensity of the PI stain. **(C)** Surface and total vimentin expression during G1, S and G2 phase. Surface staining and total vimentin stain was carried out as described in **(A)**. Light gray histogram: whole cell population; black histogram: cells gated for G1 population; dark gray histogram: cells gated for S phase; white histogram: cell gated for G2. Triplicates were analyzed; the average and standard deviation of vimentin and the respective secondary antibody-only controls (2^) are shown. **(D)** Cells were synchronized in the early S phase (inset shows a schematic of cell cycle) using a double thymidine block and collected at different time points (0, 4, 6, 8 and 16 h) after release. Cells were stained for cell surface vimentin (white bars) or for CPMV uptake (black bars). Data were normalized against the respective controls (secondary antibody only for vimentin staining, and primary and secondary antibody only for CPMV uptake studies). All experiments were carried out in duplicates or triplets and repeated at least twice; average and standard deviations are shown. For all experiments, at least 10,000 events gated for single and live cells were recorded and data were analyzed using FlowJo 8.7.1 software.

CPMV: Cowpea mosaic virus; non-syn.: Non-synchronized; PI: Propidium iodide.

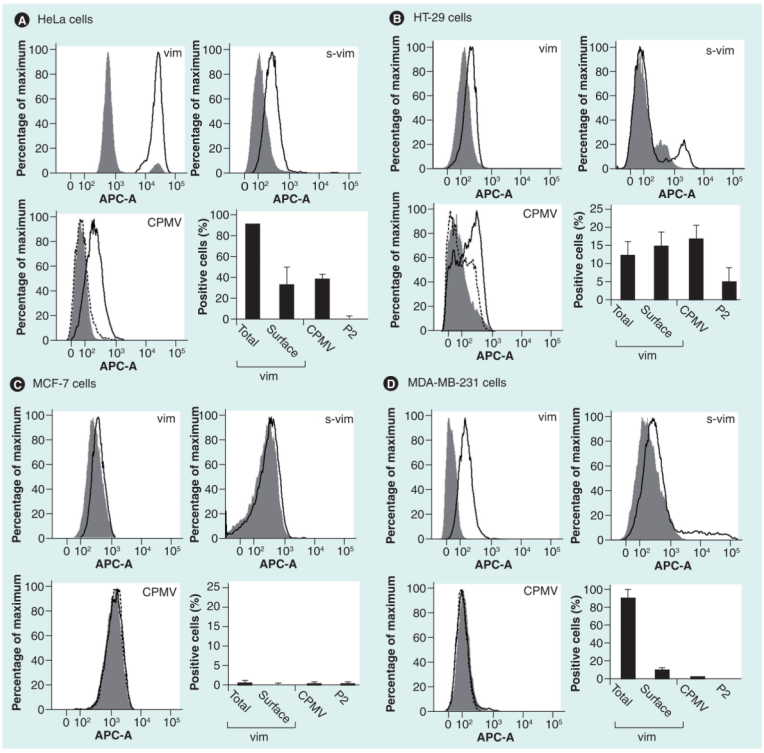

Figure 3. Comparison of surface versus total vimentin and cowpea mosaic virus nanoparticle uptake on a panel of cancer cell lines evaluated by flow cytometry

(A) HeLa cells. **(B)** HT-29 cells. **(C)** MCF-7 cells. **(D)** MDA-MB-231 cells. Cells were stained for vimentin using the vimentin-specific monoclonal v9 antibody. For CPMV uptake studies, native CPMV particles and PEGylated P2 particles were used, and staining was achieved using a polyclonal rabbit anti-CPMV antibody and A647-labeled goat antirabbit secondary antibody. Histograms and bar charts are shown. Gray solid histogram: secondary antibodies only. Black histogram: total vimentin (vim), s-vim or CPMV uptake. Dotted black histogram: P2 uptake. Bar charts give the statistical analysis; note the differences in the scale of the Y-axis for the different cell lines. All experiments were repeated at least twice and samples analyzed in duplicate or triplicate. At least 10,000 events gated for single and live cells were recorded and statistical analysis was performed using FlowJo 8.7.1 software. Shown is the average and standard deviation; values were normalized against the respective controls (secondary antibody only for vimentin staining, and primary and secondary antibody only for CPMV uptake studies).

APC-A: Allophycocyanin-A; CPMV: Cowpea mosaic virus; s-vim: Surface vimentin; vim: Vimentin.

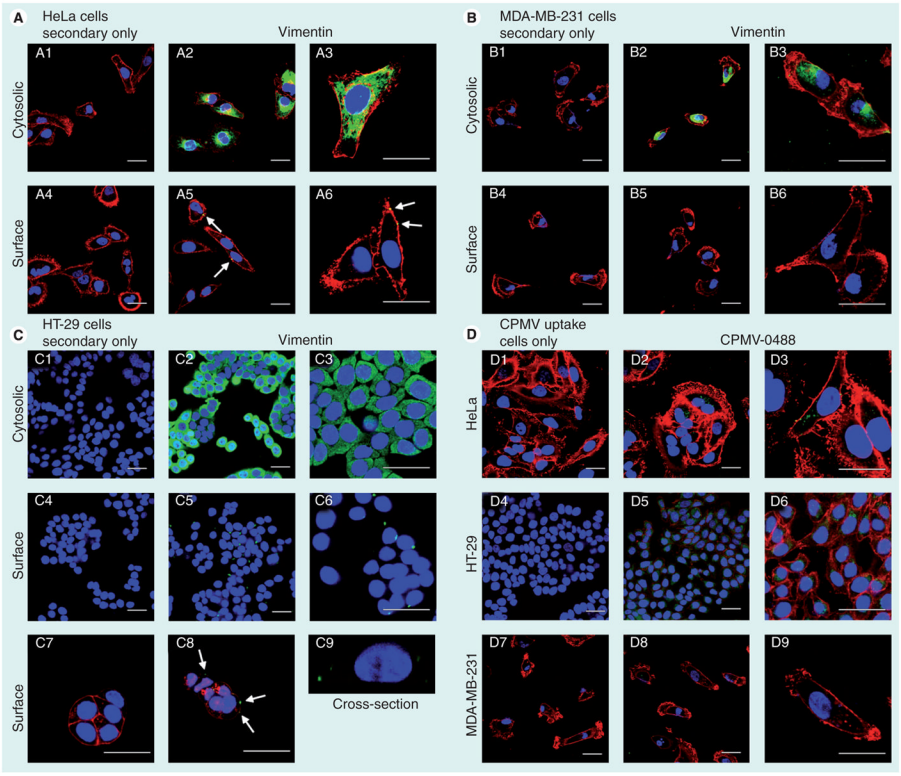

Figure 4. Levels of surface vimentin correlates to cowpea mosaic virus nanoparticle uptake by cancer cells evaluated by confocal microscopy

Cytosolic and surface vimentin expression in **(A)** HeLa, **(B)** MDA-MB-231 **(C)** and HT-29 cells. Vimentin was detected using the monoclonal antivimentin antibody v9, cells were permeabilized to stain cytosolic vimentin **(2 & 3)** and live cells staining was performed to detect surface vimentin **(5 & 6)**. Secondary antibody only controls are shown **(1 & 4)**. Color-coding: red: WGA-A555 (cell membrane); green: vimentin; blue: DAPI (nucleus). The scale bar is 30 μm. Arrows in panels, **A5, A6 & C8** point at surface vimentin. **C9** shows a cross-section through a cell. Z-sections were recorded at a step size of 0.3 μm. The section comprises four frames and is 1.2 μm deep. **(D)** CPMV-O488 particles were used for nanoparticle uptake studies. Color coding: red: WGA-A555 (cell membrane); green: CPMV; blue: DAPI (nucleus). The scale bar is 30 μm. Imaging was performed using a Biorad 2100 confocal microscope with a 60× oil objective. Data were analyzed and images were created using ImageJ [101].

CPMV: Cowpea mosaic virus.

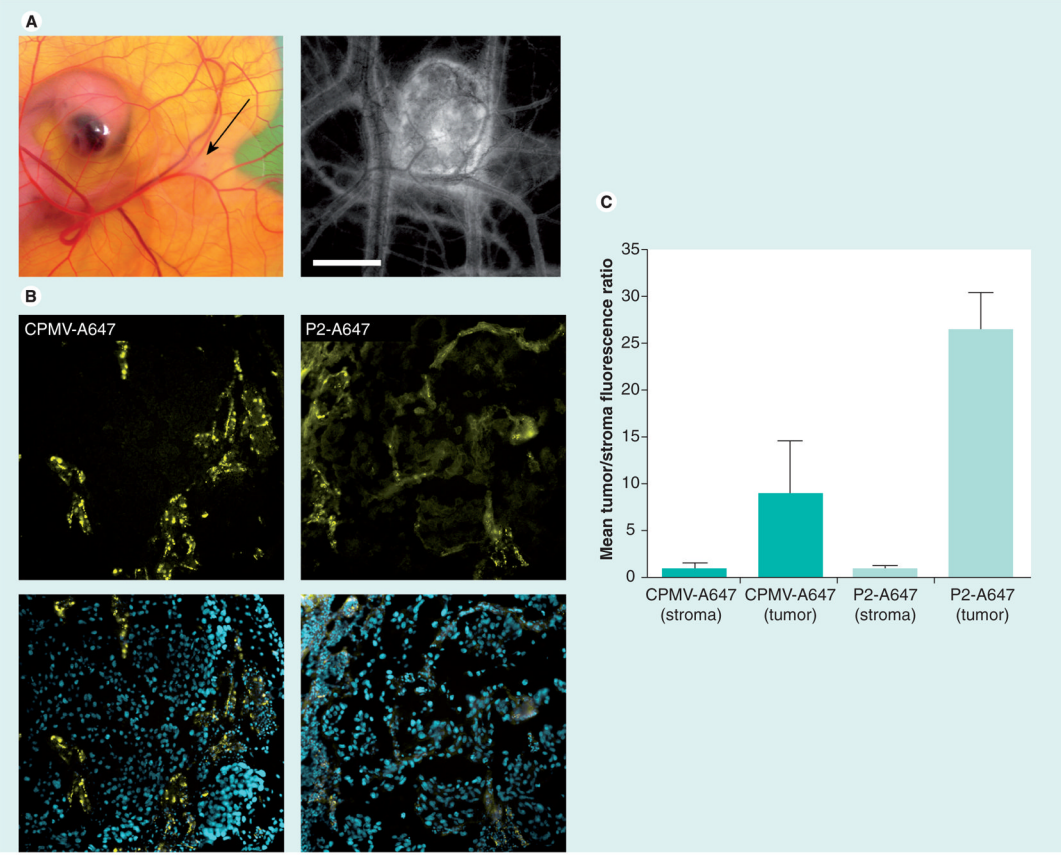

Figure 5. Uptake of cowpea mosaic virus in human tumor xenografts in the chorioallantoic membrane

(A) Human HT-29 tumors were implanted in the chorioallantoic membrane of a shell-less chicken embryo. Black arrow indicates tumor (left). Tumor size and vascularity were assessed using intravital imaging after intravenous injection of fluorescein-dextran (right). Scale bar: 3 mm. **(B)** Fluorescence confocal imaging of tissue sections from HT-29 tumor excised 6 h after injection with either CPMV-A647 or P2-A647 (yellow: CPMV/P2; blue: DAPI). **(C)** Quantification of mean A647 fluorescence in tissue sections corresponding to nontumor stroma and tumor in embryos injected with either CPMV-A647 or P2-A647. CPMV-A647 uptake in tumor is 8.9-times that of surrounding nontumor stroma. P2-A647 uptake in tumor is 26.5-times that of surrounding nontumor stroma.
CPMV: Cowpea mosaic virus.